ACS APPLIED NANO MATERIALS

www.acsanm.org Article

Graphene Foam Current Collector for High-Areal-Capacity Lithium–Sulfur Batteries

Fengjiao Liu, Shailendra Chiluwal, Anthony S. Childress, Christopher Etteh, Kymani Miller, Marlena Washington, Apparao M. Rao, and Ramakrishna Podila*

Cite This: *ACS Appl. Nano Mater.* 2021, 4, 53–60 Read Online

ACCESS | Metrics & More | Article Recommendations | Supporting Information

ABSTRACT: Extending lithium–sulfur battery (LSB) electrode architecture into three dimensions (3D) has been proposed for more than a decade. A 3D lightweight and porous current collector that is capable of holding high amounts of sulfur (S) without any significant decrease in performance has been elusive. Although many material solutions (such as sulfurized polyacrylonitrile or SPAN) have been identified for alleviating polysulfide formation and the so-called shuttle effect, their incorporation into 3D current collectors with high capacity at the electrode level has not yet been realized. Here, we show that graphene foams (GFs) are ideally suited as 3D lightweight current collectors for LSBs and outperform the conventional carbon-coated Al (Al/C) foils at the electrode level. Specifically, we demonstrate that the open framework of GFs facilitates high mass loading of SPAN without any deterioration in capacity at the active material level even at high S loading. At the electrode level, GF-SPAN cathodes exhibited capacities of ∼200 mAh $g^{-1}_{electrode}$ at 0.1C even with low S loadings (∼1.1 mg cm^{-2}), which is at least 3 times higher than conventional Al/C electrodes. More importantly, we fabricated cells with a high mass loading of 26.5 mg cm^{-2} S by stacking multiple GFs to achieve an areal capacity as high as ∼20 mAh cm^{-2} (at a current density of 3.0 mA cm^{-2} up to 50 cycles), which is at least 3 times higher than LSB areal capacity (6 mAh cm^{-2}) needed to displace LIBs.

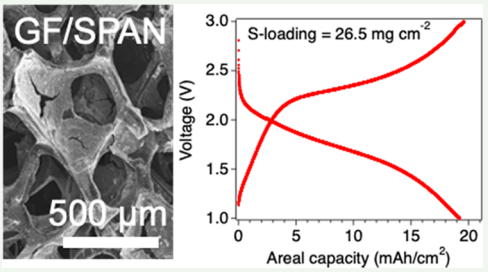

KEYWORDS: *lithium–sulfur batteries, graphene, three-dimensional current collectors, energy storage, lithium-ion batteries*

INTRODUCTION

Despite the advances in Li-ion batteries (LIBs), there is a great need for cheaper, safer, and lightweight batteries for many applications including electrical vehicles (EVs).[1] In EVs, automotive battery packs typically consist of a large number of LIBs (hundreds to thousands) to meet the required power and capacity needs of an electric vehicle. The energy density of state-of-the-art LIBs (∼250 Wh kg^{-1} at the cell level for a 18650 cell) is nearing its practical limit due to the limited capacity of presently used Li-ion-insertion cathodes (e.g., lithium nickel manganese cobalt oxide or NMC, lithium nickel cobalt aluminum oxide battery or NCA, etc.).[2,3] Unlike other Li-insertion cathodes, elemental sulfur (S) is an excellent cathode active material because it has a high theoretical lithium capacity of 1675 mAh g^{-1}.[4] Indeed, the last decade witnessed a great interest in lithium–sulfur batteries (LSBs) because their theoretical energy density is over 5 times larger than that of conventional LIBs based on intercalation electrodes. S is also much less expensive, more abundant, and environmentally friendly than the metal oxides that are currently used as standard LIB cathodes. Though S is a promising material, the practical realization of LSBs has been impeded by several challenges such as: (i) low electronic conductivity of S that necessitates a high fraction of conductive additives, (ii) the formation and dissolution of higher-order polysulfides (LiS_x, $4 \leq x \leq 8$) by the electrolyte and subsequent capacity fade due to loss of active material,[5−7] (iii) unstable solid–electrolyte interface (SEI) layer[8] and the passivation of the lithium metal anode with insoluble lithium sulfide[9] (e.g., Li_2S/Li_2S_2), and (iv) poor electrical contact between the active material and current collector, particularly at high S loading.[10] Drastic improvements in the current collector and electrode architecture of LSBs are also imperative to achieve an areal capacity of 6 mAh cm^{-2} (operating at 2.1 V), which is the lower threshold necessary for LSBs to displace commercial LIBs.[11]

To overcome such limitations (described in challenges (i)–(iv)), hierarchical electrode architectures have been explored;[5,12−14] for example, to mitigate poor electrical conductivity issues (challenge (i)) and polysulfide migration (challenge (ii)), researchers developed composite cathodes wherein elemental S was encapsulated in polymers or porous carbon matrices.[15−18] Although the physical confinement of S

Received: August 2, 2020
Accepted: December 15, 2020
Published: January 7, 2021

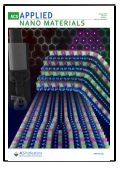

https://dx.doi.org/10.1021/acsanm.0c02073
ACS Appl. Nano Mater. 2021, 4, 53–60

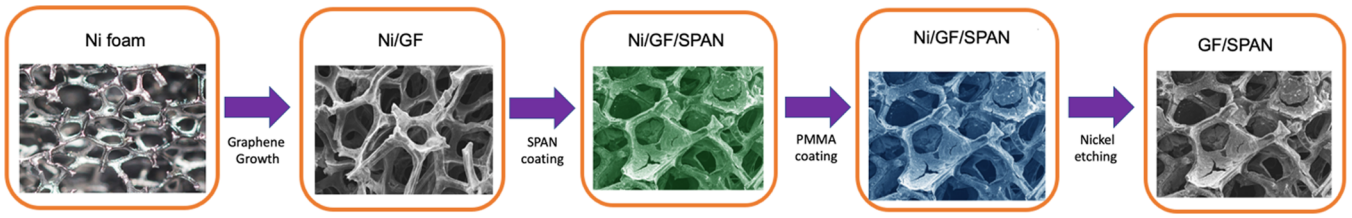

Figure 1. Schematic showing the fabrication steps of a GF/SPAN cathode: A graphene foam (GF) is grown on a 3D-Ni mesh using the chemical vapor deposition technique. The GF/SPAN cathode electrode was prepared by vacuum filtrating a slurry of SPAN, carboxymethyl cellulose, and carbon black (mass ratio of 70:15:15) onto the GF current collector (with Ni mesh). The as-prepared cathode electrode was air-dried overnight followed by drying in an oven ∼130 °C for 12 h. Next, 5 wt % poly(methyl methacrylate) (PMMA) thin layer was coated on the cathode before it was submerged in a 6 M HCl solution for 6 h at 70 °C to completely remove the nickel. The resulted cathode electrode was cleaned in KOH solution and washed in DI H_2O and dried.

within the pores was found to be effective in reducing the outward diffusion of polysulfides, the weak interaction between nonpolar carbon and polar polysulfides proved insufficient to completely eliminate the shuttle problem. An alternative to S composite cathodes are sulfurized polymers, wherein the S is bound to a conjugated polymer backbone.[19] In a sulfurized polymer, S is not present in its elemental state S_8 and thus such polymers circumvent the formation of higher-order polysulfides that are often observed when S_8-based cathodes are used (challenge (ii)). Moreover, sulfurized polymers are easy to produce in large quantities and can be incorporated into typical slurry formulations that are compatible with current manufacturing equipment used by the industry. In 2002, Wang et al.[20,21] synthesized sulfurized polyacrylonitrile (SPAN) for use in LSBs, which exhibited a gravimetric capacity of ∼800 mAh g^{-1},[22−28] and since then SPAN has been regarded as the standard for sulfurized polymer cathodes. Sixteen years later, another group[29] proposed that the polysulfide shuttle is mitigated by SPAN cathodes since the lithium-ion complexes with negative S ions along the polymer backbone and thereby mitigates the formation of free polysulfides.[25] As mentioned earlier, higher-order polysulfides have not been observed to form in SPAN as S is not present in its elemental S_8 form. SPAN also reacts favorably with typical electrolyte components to form a stable SEI layer. Fan et al.[30] demonstrated that certain electrolyte blends could simultaneously form an SEI layer on both the SPAN-based cathode and Li anode (challenge (iii)).

The conventional current collector for cathodes in LIBs and LSBs is a 10−25 μm thick aluminum foil, which accounts for 30−50% of the electrode weight. Furthermore, carbon-coated Al (Al/C) current collectors cannot support thick layers of the active material as they easily develop cracks in addition to resulting in longer diffusion paths for ions within the layer.[31] They are also prone to oxidation and corrosion during cycling, which often electrically delaminates the active material layer from the current collector ensuing in the high internal resistance of the battery.[32] Due to the abovementioned reasons, achieving high areal capacity using conventional current collector has been challenging.

Extending battery electrode architecture into three dimensions (3D) has been proposed for more than a decade.[33] The ideal electrode structure consists of both 3D percolating electron and ion pathways with short transport distances. Current collectors with conductive open frameworks are capable of binding the active material within them and have been shown to support enhanced cell cyclability for various rechargeable battery systems including LSBs.[34−40] Specifically, different metal foams and composites (Al, Ni,[34] Ni/carbon fiber,[36] Al/carbon nanotube,[37] etc.) have been used to improve the cycle stability of LSBs. While metal foams provide excellent electrical conductivity, they also significantly reduce the energy density at the electrode level due to their weight. Conversely, lightweight porous current collectors such as nanocellulose fibers or cotton[39] are not conductive enough to support fast charge transport. Ideally, a current collector of this type should be lightweight, porous, mechanically robust, electrically conducting, support high S loadings up to >15 mg cm^{-2}, and exhibit long-term cycle stability. Although 3D porous current collectors reported thus far[32,34−40] achieve one or more of these attributes, an ideal 3D current collector to fabricate a high energy and power density battery beyond the simple microbatteries is still needed.[41] In this study, we build upon our recent LSBs, which were prepared using (i) aqueous SPAN slurry formulations, (ii) aluminum foils, and (iii) a mixed electrolyte formulation which supported bilateral SEI formation,[30] to fabricate LSBs using a lightweight and electrically conductive 3D graphene foam (GF) with SPAN as the active material. The porous framework of GF accommodates a higher loading of active material (up to a S loading of 26.5 mg cm^{-2} or a SPAN loading of ∼76 mg cm^{-2}) without the need for additional binders (beyond ∼15 wt % binder that is typically used during preparation of the slurry). Such a high mass loading of 26.5 mg cm^{-2} yielded an areal capacity of 19.2 mAh cm^{-2} at a current density of 3.0 mA cm^{-2} up to 50 cycles.

RESULTS AND DISCUSSION

A GF/SPAN current collector was prepared using the chemical vapor deposition technique and vacuum filtration (Figure 1). Detailed information regarding the preparation of GF and SPAN can be found in the Experimental Section and in the Supporting Information (Figures S1−S3). As shown in Figure 2a, the GF current collector has an open macroporous structure that is ideally suited for accommodating a high loading of active material. The active material slurry is composed of SPAN, carboxymethyl cellulose, and Super-P conductive carbon with a mass ratio of 70:15:15. The aqueous slurry was made to fill the open structure of the GF current collector by vacuum infiltration (Figure 2c−f). Despite the presence of cracks (indicated by arrows in Figure 2c,e) in the infiltrated GF-SPAN, the macroporous structure of the GF facilitated good electrical contact within SPAN. Indeed, as it will be discussed later in Figures 6 and 7, such a porous structure and electrical connectivity within GF-SPAN is retained even after 100 cycles at 0.1C. As-prepared GF1 and GF2 cathodes (Figure 2c−f) accommodated a S loading of 1.1

https://dx.doi.org/10.1021/acsanm.0c02073
ACS Appl. Nano Mater. 2021, 4, 53−60

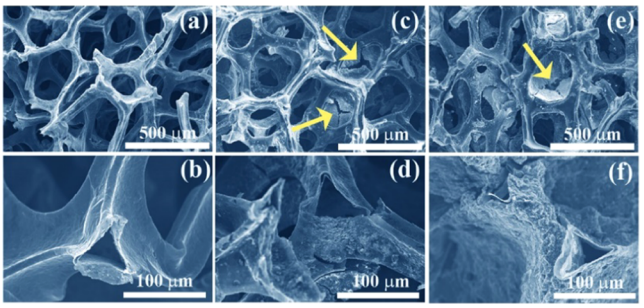

Figure 2. Scanning electron microscopy images showing freestanding GF cathodes. (a, b) Pristine GF; (c, d) GF1 cathode with 1.1 mg cm^{-2} S loading; and (e, f) GF2 cathode with 2.1 mg cm^{-2} S loading. The arrows in (c) and (e) show cracks present in the infiltrated SPAN. Despite the presence of such cracks in SPAN, GF supports good electrical connectivity within SPAN.

and 2.1 mg cm^{-2} (i.e., SPAN loading of 3.1 and 6.0 mg cm^{-2}), respectively. It must be acknowledged that in much of the literature for LSBs, the performance is often normalized by the mass of S. In this study, the total S mass in SPAN and thus the electrode was ascertained using traditional CHNOS measurements (see Table S1). By adjusting the slurry concentration and stacking multiple GFs together in coin cells, a high mass loading of S up to 26.5 mg cm^{-2} was achieved in this study.

To highlight the advantage of using GF current collectors, the SPAN slurry was also coated on conventional Al/C foils (i.e., Al foil with an overcoat of sp^2 carbon) via a doctor blade (labeled Al/C1 and Al/C2, which revealed a net S loading of 0.1 and 0.3 mg cm^{-2}, respectively). As mentioned above, the Al/C current collectors were only able to support a maximum S loading of 0.3 mg cm^{-2} without developing cracks (see Figure S4). Table S2 lists the S loading for all samples used in this study along with the sample labels used for the discussion below.

Electrochemical Performance. To evaluate the electrochemical performance, cyclic voltammetry (CV) was performed on GF1 and GF2 at a scan rate of 0.1 mV s^{-1} (Figure 3). CV curves for other scan rates are presented in Figure S5, and for comparison, sample Al/C1 was also tested under identical conditions. Figure 3a,b shows the gravimetric capacities of GF0, GF1, GF2, and Al/C1 electrodes at the S and electrode levels, respectively. The CV data of a typical LSB with elemental S cathode shows the presence of two reduction peaks at 2.3 and 2.0 V, the former corresponds to the reduction of S (S_8) to higher-order lithium polysulfides (Li_2S_x, $4 \leq x \leq 8$) and the latter to the subsequent formation of insoluble Li_2S_2/Li_2S.[42,43] As expected, SPAN did not exhibit these reduction peaks because it does not contain S in its elemental form. However, two distinct peaks at 2.0 and ∼1.7 V are evident in the CV data of all SPAN electrodes (Figure 3a,b). This set of peaks correspond to the transformation from short-chain sulfur to Li_2S (SPAN-S_x^- + $2Li^+$ + $2e^-$ ↔ SPAN-S_{x-1}^- + Li_2S; $2 \leq x \leq 7$). It should be mentioned that recently in $Se_{0.06}$SPAN similar reduction peaks were observed but the transformation of short-chain sulfur was suggested to be mediated through to the fast reduction of soluble Li_2S_n ($n \leq 4$) to insoluble Li_2S_2/Li_2S.[44,45]

Figure 3a,b shows cyclic voltammograms for GF0, GF1, GF2, and Al/C1 normalized by the weight of S and the weight of the cathode, respectively. As seen in Figure 3a, Al/C1 appears to be superior to GF0 when normalized by the mass of S. This observation is attributed to lower thickness of SPAN coating on Al/C1 compared to GF0. Although such a lower thickness in Al/C1 foil naturally facilitates better access to Li ions, increasing the S loading beyond 0.3 mg cm^{-2} without delamination is highly difficult. A typical Nyquist plot is shown in Figure 3c in which the first semicircle is due to the SEI layer and the second semicircle is due to charge transfer at the electrolyte and electrode interface.[46−52] Modeling the Nyquist plot with the Randles circuit shown in Figure S6, the

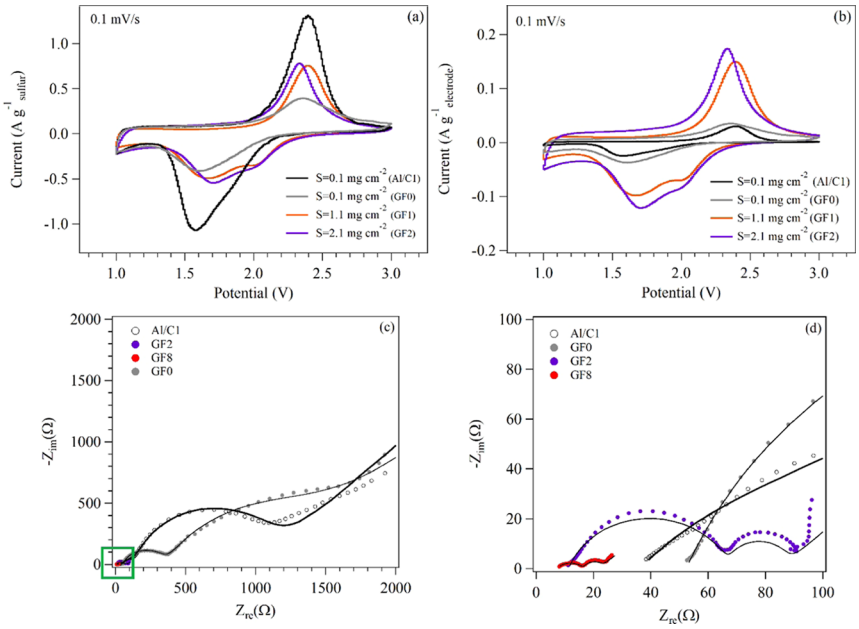

Figure 3. Cyclic voltammograms for GF1, GF2, and Al/C1 normalized by the weight of S (a) and the weight of the cathode (b). Nyquist plot of Al/C1, GF0, GF1, and GF8 after the fifth discharge cycle (c). An expanded view of the green boxed region in (c) is shown in (d). The solid lines in (c) and (d) represent the fits obtained using the circuit shown in Figure S6.

https://dx.doi.org/10.1021/acsanm.0c02073
ACS Appl. Nano Mater. 2021, 4, 53−60

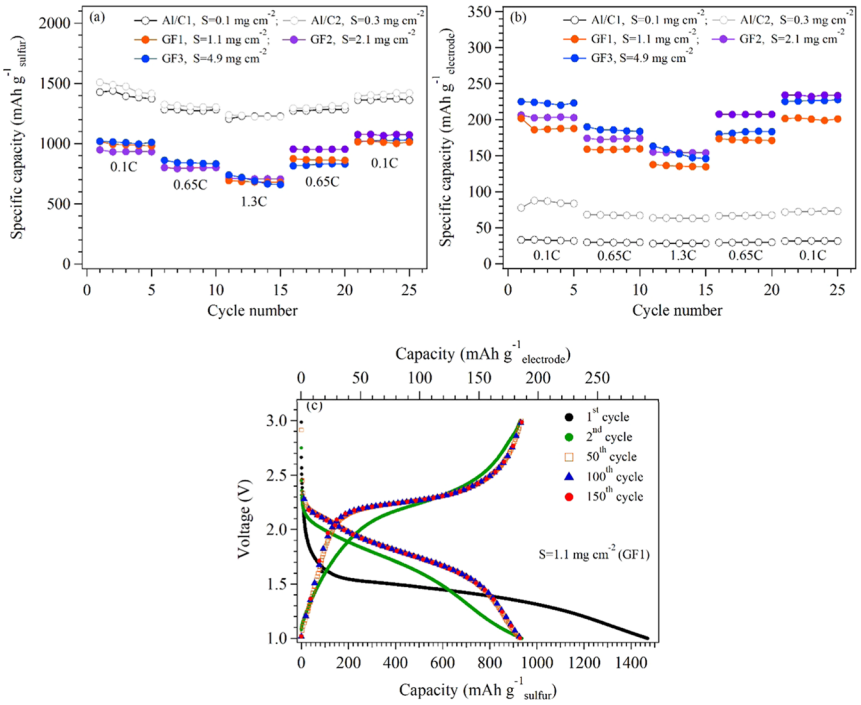

Figure 4. Specific capacity normalized by the weight of S (a) and the electrode (b) at 0.1, 0.65, and 1.3C for Al/C1, Al/C2, and GF1−GF3. The S loadings are indicated in the figure. (c) Charge/discharge curves for GF1 normalized by the weight of S and the weight of electrode (panel c, 220 mA g^{-1}_{sulfur}, and 45 mA $g^{-1}_{electrode}$).

resistances for each electrode were deduced and are listed in Table S3. The series (R_s) and SEI (R_{SEI}) resistances of the GF0 cathode were found to be higher than that of Al/C1 and attributed to unfilled pores in GF0 because of the low SPAN loading of 0.1 mg cm^{-2}. With higher S loading, the values of R_s, R_{SEI}, and charge transfer resistance (R_{CT}) decreased as evident in Figure 3c,d and Table S3.

We further investigated the possibility of increasing the S loading, and the rate performance of GFs at 0.1, 0.65, and 1.3C. Figure 4a,b shows the rate capacity at the S and electrode levels, respectively. For comparison, Al/C1 and Al/C2 were also tested at the same current rates. Although the rate capacity at the S level is conventionally reported in publications, the rate capacity at the electrode level is more relevant for practical applications. At 0.1C, the discharge capacity of GF1−GF3 was found to be ∼900−1000 mAh g^{-1}_{sulfur} despite a wide range of S loadings from 1.1 to 4.9 mg cm^{-2}; this observation highlights that the porous GF current collector can accommodate a high S loading without much deterioration in capacity. The GF cathodes were able to deliver capacities of ∼700 mAh g^{-1}_{sulfur} even at 1.3C. A stable discharge capacity of 900−1000 mAh g^{-1}_{sulfur} was recovered when the C-rate was restored to 0.1C (after 5 cycles at 1.3C), highlighting the excellent stability of the GF cathodes prepared in this study. At the S level, both Al/C1 and Al/C2 exhibited a higher rate capacity of ∼1400 mAh g^{-1}_{sulfur}. However, at the electrode level, the GF cathodes exhibited capacities of ∼200 mAh $g^{-1}_{electrode}$ at 0.1C, which is 3 times higher than that of Al/C1 and Al/C2 (∼30 and ∼70 mAh $g^{-1}_{electrode}$, respectively). Additionally, at 0.65 and 1.3C, the capacities of GF1−GF3 cathodes at the electrode level are higher than those of Al/C1 and Al/C2. Next, we evaluated the cycling stability and Coulombic efficiency of GF1−GF3 up to 150 cycles at 0.1C (Figure S7) and up to 500 cycles for GF2 at 1C (Figure S8). As an example, the galvanostatic cycling data of GF1 (1C = 1675 mA g^{-1}_{sulfur}) are shown in Figure 4c. The bottom (/top) x-axis label corresponds to the specific capacity normalized to the weight of S (/electrode). The initial discharge of GF1 yields a large irreversible capacity due to the formation of the bilateral SEI layer as reported in our previous publication.[30] Following the initial discharge, the GF1 cathode showed an excellent cycle stability up to 150 cycles with no loss in capacity, demonstrating the stability of SPAN/GF electrode at 0.1C. A typical scanning electron microscope (SEM) image of the GF3 electrode taken after 100 cycles is shown in Figure S9. Clearly, the GF is compressed compared to its original state, which is unavoidable due to crimping during the fabrication of the coin cell. Nonetheless, the GF served as an excellent electrode, which is evident from the electrochemical performance. It should be mentioned that we could not evaluate the rate performance for higher S loading as our battery testing unit was limited to a maximum current of 10 mA. Hence, as discussed below, we focused on evaluating the areal capacity of our GF-SPAN cathodes with higher S loadings up to 26.5 mg cm^{-2}.

Figure 5 illustrates the areal capacity of all GF and Al/C1 cathode up to 50 cycles at a current density of 3 mA cm^{-2}. Al/C1 and GF1−GF5 delivered areal capacities of 0.13, 0.8, 1.9, 4.3, 6.7, and 9.3 mAh cm^{-2}, respectively. As mentioned in the introduction, an areal capacity of 6 mAh cm^{-2} is required for LSBs to compete with LIBs. While we were able to achieve >6 mAh cm^{-2} capacity with GF4 and GF5 electrodes, we also prepared GF6−GF8 cathodes with a S loading as high as 26.5 mg cm^{-2}, which exhibited an even greater areal capacity of ∼19.2 mAh cm^{-2}. As evident from Table S5, the performance of GF-SPAN electrodes is comparable with other recently published articles in the literature.

Lastly, we performed detailed elemental mapping using energy-dispersive X-ray spectroscopy to understand the

https://dx.doi.org/10.1021/acsanm.0c02073
ACS Appl. Nano Mater. 2021, 4, 53−60

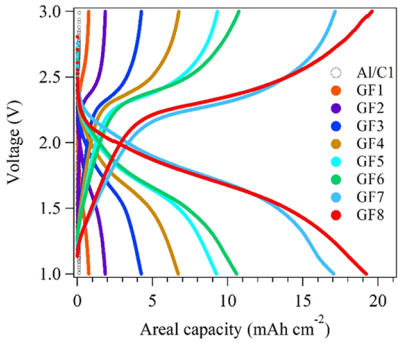

Figure 5. Charge/discharge profiles for all GF-SPAN and Al/C1 cathodes at the 50th cycle at an areal current density of 3 mA cm^{-2}.

mechanical stability and electrical connectivity within GF cathodes. As shown in Figure 6 and 7 we found that GF

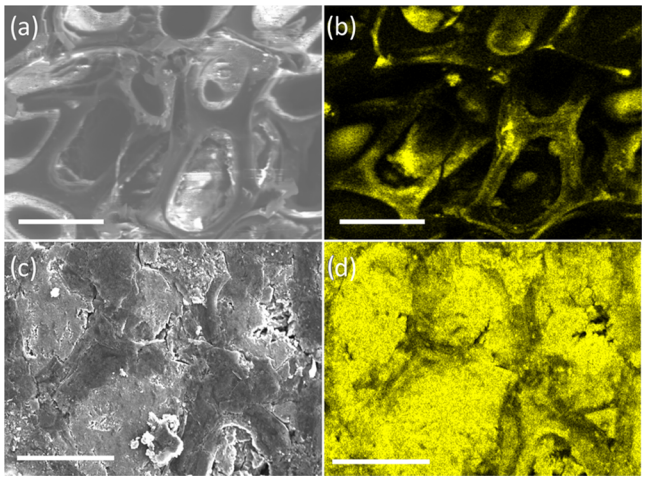

Figure 6. Top-view electron micrographs and energy-dispersive X-ray elemental maps for GF-SPAN cathodes after 0 (a, b) and 100 cycles (c, d). Sulfur is shown in yellow color. Clearly, the porous structure of GF is retained even after 100 cycles (see also cross-sectional images in Figure 7), suggesting that GF is a mechanically robust 3D current collector. All scale bars are 100 μm.

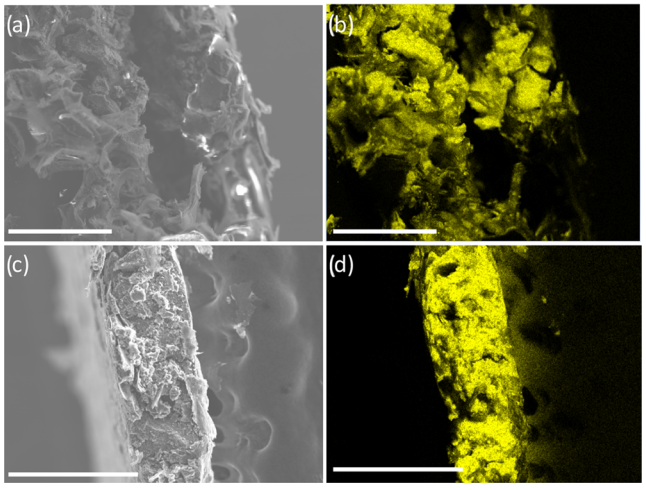

Figure 7. Cross-sectional electron micrographs and energy-dispersive X-ray elemental maps for GF-SPAN cathodes after 0 (a, b) and 100 cycles (c, d). Sulfur is shown in yellow color. All scale bars are 250 μm.

cathodes retained their physical foam structure and appearance even after 100 cycles suggesting that GFs are mechanically robust. Furthermore, GF was found to facilitate electrical connectivity among SPAN domains through its three-dimensional foam framework after 100 cycles, unlike a flat Al current collector. Such an observation concurs with the Nyquist plots (cf. Figure 3c,d) that show much lower resistance for GF-based cathodes.

CONCLUSIONS

In summary, we demonstrated that GF-SPAN electrodes support high S loading for high-areal-capacity LSBs. Specifically, GF8 exhibited an areal capacity of ~20 mAh cm^{-2} at 3 mA cm^{-2} with a S loading of 26.5 mg cm^{-2}, which is one-third the weight of S used in previous studies for achieving similar areal capacity. GF-SPAN cathodes also show an excellent cycle stability up to 150 cycles with no loss in capacity at 0.1C. The superior performance of GF-SPAN electrodes is attributed to the excellent electrical contact between the active material and the host GF, particularly at high S loading. This study highlights that a proper choice of a current collector can facilitate higher S loading, leading to higher areal capacity.

EXPERIMENTAL SECTION

Chemicals and Materials. Lithium bis (trifluoromethane) sulfonamide (LiTFSI), ethylene carbonate (EC), 1,2-dimethoxyethane (DME), 1,3-dioxolane (DOL), and polyacrylonitrile (PAN) were purchased from Sigma-Aldrich. The sulfur (S) powder (325 mesh) was purchased from Alfa Aesar. The Ni-foam (95% porosity) and carbon-coated Al foil were purchased from MTI. The thickness of carbon-coated Al foil is 18 μm.

Preparation of an Electrolyte. Typically, 1 M LiTFSI in $EC_{0.5}DME_{0.25}DOL_{0.25}$ electrolyte was employed in this study since it is the optimized electrolyte for a SPAN cathode and promotes the simultaneous formation of bilateral SEI layers on both the SPAN (S-host) cathode and lithium anode shown in our previous study.[30] The amount of electrolyte plays an important role for porous current collectors. As is well known, the amount of the electrolyte must be increased in proportion to the sulfur loading; in other words, the higher the sulfur loading, a higher amount of electrolyte will be needed. In this regard, our study is meritorious because only 7 μL mg^{-1}_{sulfur} of electrolyte was needed for all GF-based cells discussed in our study, which is probably the lowest amount reported for any porous electrode.

Synthesis of a Graphene Foam (GF) Current Collector. Few-layer graphene was grown on nickel foams through a traditional chemical vapor deposition (CVD) method using a 1 in. tube furnace. The nickel foam was annealed at 900 °C under Ar and H_2 atmosphere for an hour before the growth to remove any surface oxides. Then, the furnace was cooled to 850 °C with a cooling rate of 10 °C min^{-1}. Subsequently, the few-layer graphene was grown under a gas flow rate of 230 sccm Ar, 120 sccm H_2, and 100 sccm CH_4 for an hour. The flow of methane was halted, and the furnace was cooled and held at 400 °C for 2 h. Finally, the furnace was cooled to room temperature under Ar flow.

Preparation of a Cathode Electrode. Sulfurized polyacrylonitrile (SPAN) was synthesized in a N_2 atmosphere at 450 °C. The temperature of the furnace was slowly raised at 5 °C min^{-1} and kept at 450 °C for 6 h. The initial mass ratio of elemental S and polyacrylonitrile (PAN, M_w = 150 000) is 3:1. The GF cathode electrode was prepared by vacuum filtrating a slurry of SPAN, carboxymethyl cellulose, and carbon black (mass ratio of 70:15:15) onto the GF current collector. The as-prepared cathode electrode was air-dried overnight followed by drying in an oven ~130 °C for 12 h. Next, 5 wt % PMMA thin layer was coated on the cathode before it was submerged in a 6 M HCl solution for 6 h at 70 °C to completely remove the nickel. The resulted cathode electrode was cleaned in

https://dx.doi.org/10.1021/acsanm.0c02073
ACS Appl. Nano Mater. 2021, 4, 53−60

KOH solution and washed in DI H_2O and dried. For Al/C electrode, the same slurry was coated on Al/C using a doctor blade and followed by the same drying procedure. Ten millimeter coupon was punched out and used as the cathode.

Material Characterization. Thermogravimetric analysis (TGA) was performed in N_2 from room temperature to 800 °C with a heating rate of 20 °C min^{-1} using an STA 449 Jupiter (NETZSCH) thermogravimetric. S content in SPAN was measured using an elemental analyzer (Thermo Scientific-FlashEA 1112 series). The X-ray photoelectron spectroscopy (XPS) analysis was performed with Kratos Axis Supra XPS (X-ray source: monochromated Al Kα, multichannel plate, and delay line detector with a take-off angle of 90°). The analyzer was operated in fixed analyzer transmission (FAT) mode with survey scans taken with a pass energy of 160 eV and high-resolution scans taken with a pass energy of 20 eV. SPAN spectra were recorded under charge neutralization conditions using a low-energy electron gun within the field of the magnetic lens. The resulting spectra were processed using CasaXPS software. Quantachrome Autosorb iQ was used to measure the surface area of the graphene foam and the cathode electrode. Scanning electron microscopy (Hitachi SEM-4800) was employed to characterize the microstructure of SPAN and as-coated GFs. S distribution energy-dispersive X-ray spectroscopy (EDS) was used to obtain the S distribution in SPAN powder. A Renishaw inVia Raman microscope system was used for characterizing the Raman spectra of SPAN. To obtain the real-time electrochemical environment and bonding information during the charge/discharge process, the acquisition time was 10 s per spectrum with two accumulation for each spectrum.

Electrochemical Characterization. The LiS half cells were assembled in the glovebox using solid Li chips as the anode. The galvanostatic charge/discharge was measured using a voltage range of 1.0−3.0 V vs Li/Li^+ and all gravimetric capacity was normalized by mass of S and mass of the cathode (which consists of SPAN, CMC binder, carbon black, and the current collector), respectively. The areal capacity calculations were normalized by the two-dimensional area of the cathode. Electrochemical testing was carried out using a Gamry 3000 potentiostat. Cyclic voltammetry (CV) measurements were performed at various scan rates (0.1, 0.2, 0.5, 0.8, 1 mV s^{-1}) with a voltage range of 3.0−1.0 V. The electrochemical impedance spectra (EIS) measurements were conducted at room temperature in the frequency range of 100 kHz to 0.01 Hz in galvanostatic mode with a root-mean-square alternating current of 1C as excitation signal. To ensure equal conditions, cells were measured in the discharged state after the fifth cycle between 3 and 1 V at 0.1C.

■ ASSOCIATED CONTENT

Supporting Information

The Supporting Information is available free of charge at https://pubs.acs.org/doi/10.1021/acsanm.0c02073.

Detailed physical, chemical, and electrochemical characterizations of SPAN, graphene foam, and GF-SPAN cathodes (PDF)

■ AUTHOR INFORMATION

Corresponding Author

Ramakrishna Podila − *Department of Physics and Astronomy, Clemson Nanomaterials Institute, Clemson University, Anderson, South Carolina 29625, United States; Laboratory of Nano-Biophysics, Clemson University, Clemson, South Carolina 29634, United States;* orcid.org/0000-0003-0472-2361; Email: rpodila@clemson.edu

Authors

Fengjiao Liu − *Department of Physics and Astronomy, Clemson Nanomaterials Institute, Clemson University, Anderson, South Carolina 29625, United States*

Shailendra Chiluwal − *Department of Physics and Astronomy, Clemson Nanomaterials Institute, Clemson University, Anderson, South Carolina 29625, United States; Laboratory of Nano-Biophysics, Clemson University, Clemson, South Carolina 29634, United States;* orcid.org/0000-0003-3556-2938

Anthony S. Childress − *Department of Physics and Astronomy, Clemson Nanomaterials Institute, Clemson University, Anderson, South Carolina 29625, United States*

Christopher Etteh − *Department of Chemistry, Claflin University, Orangeburg, South Carolina 29115, United States*

Kymani Miller − *Department of Chemistry, Claflin University, Orangeburg, South Carolina 29115, United States*

Marlena Washington − *Department of Chemistry, Claflin University, Orangeburg, South Carolina 29115, United States*

Apparao M. Rao − *Department of Physics and Astronomy, Clemson Nanomaterials Institute, Clemson University, Anderson, South Carolina 29625, United States;* orcid.org/0000-0002-1450-3499

Complete contact information is available at: https://pubs.acs.org/10.1021/acsanm.0c02073

Notes

The authors declare no competing financial interest.

■ ACKNOWLEDGMENTS

This work was financially supported by SC-GEAR (MADE in SC) 19-GE01, the NASA-EPSCoR award under #NNH17ZHA002C, and the South Carolina EPSCoR/IDeA Program under Award #18-SR03.

■ REFERENCES

(1) *USCAR: Energy Storage System Goals*; 2015.

(2) Jung, R.; Metzger, M.; Maglia, F.; Stinner, C.; Gasteiger, H. A. Oxygen Release and Its Effect on the Cycling Stability of $LiNi_xMn_yCo_zO_2$ (NMC) Cathode Materials for Li-Ion Batteries. *J. Electrochem. Soc.* **2017**, *164*, A1361−A1377.

(3) Purwanto, A.; Yudha, C. S.; Ubaidillah, U.; Widiyandari, H.; Ogi, T.; Haerudin, H. NCA Cathode Material: Synthesis Methods and Performance Enhancement Efforts. *Mater. Res. Express* **2018**, *5*, No. 122001.

(4) Zhu, J.; Zou, J.; Cheng, H.; Gu, Y.; Lu, Z. High Energy Batteries Based on Sulfur Cathode. *Green Energy Environ.* **2019**, *4*, 345−359.

(5) Manthiram, A.; Fu, Y.; Su, Y. S. Challenges and Prospects of Lithium-Sulfur Batteries. *Acc. Chem. Res.* **2013**, *46*, 1125−1134.

(6) Mikhaylik, Y. V.; Akridge, J. R. Polysulfide Shuttle Study in the Li/S Battery System. *J. Electrochem. Soc.* **2004**, *151*, A1969−A1976.

(7) Qin, X.; Wang, X.; Xie, J.; Wen, L. Hierarchically Porous and Conductive $LiFePO_4$ Bulk Electrode: Binder-Free and Ultrahigh Volumetric Capacity Li-Ion Cathode. *J. Mater. Chem.* **2011**, *21*, 12444−12448.

(8) Soto, F. A.; Ma, Y.; De La Hoz, J. M. M.; Seminario, J. M.; Balbuena, P. B. Formation and Growth Mechanisms of Solid-Electrolyte Interphase Layers in Rechargeable Batteries. *Chem. Mater.* **2015**, *27*, 7990−8000.

(9) Yin, Y.; Franco, A. A. Unraveling the Operation Mechanisms of Lithium Sulfur Batteries with Ultramicroporous Carbons. *ACS Appl. Energy Mater.* **2018**, *1*, 5816−5821.

(10) Lv, D.; Zheng, J.; Li, Q.; Xie, X.; Ferrara, S.; Nie, Z.; Mehdi, L. B.; Browning, N. D.; Zhang, J. G.; Graff, G. L.; Liu, J.; Xiao, J. High Energy Density Lithium-Sulfur Batteries: Challenges of Thick Sulfur Cathodes. *Adv. Energy Mater.* **2015**, *5*, No. 1402290.

(11) Fang, R.; Zhao, S.; Sun, Z.; Wang, D. W.; Cheng, H. M.; Li, F. More Reliable Lithium-Sulfur Batteries: Status, Solutions and Prospects. *Adv. Mater.* **2017**, *29*, No. 1606823.

(12) Markevich, E.; Salitra, G.; Talyosef, Y.; Chesneau, F.; Aurbach, D. Review—On the Mechanism of Quasi-Solid-State Lithiation of Sulfur Encapsulated in Microporous Carbons: Is the Existence of Small Sulfur Molecules Necessary? *J. Electrochem. Soc.* **2017**, *164*, A6244−A6253.
(13) Dörfler, S.; Hagen, M.; Althues, H.; Tübke, J.; Kaskel, S.; Hoffmann, M. J. High Capacity Vertical Aligned Carbon Nanotube/Sulfur Composite Cathodes for Lithium−Sulfur Batteries. *Chem. Commun.* **2012**, *48*, 4097−4099.
(14) Wang, J.; Yang, G.; Chen, J.; Liu, Y.; Wang, Y.; Lao, C. Y.; Xi, K.; Yang, D.; Harris, C. J.; Yan, W.; Ding, S.; Kumar, R. V. Flexible and High-Loading Lithium−Sulfur Batteries Enabled by Integrated Three-In-One Fibrous Membranes. *Adv. Energy Mater.* **2019**, *9*, No. 1902001.
(15) Chen, S.; Huang, X.; Sun, B.; Zhang, J.; Liu, H.; Wang, G. Multi-Shelled Hollow Carbon Nanospheres for Lithium-Sulfur Batteries with Superior Performances. *J. Mater. Chem. A* **2014**, *2*, 16199−16207.
(16) Sun, Q.; He, B.; Zhang, X. Q.; Lu, A. H. Engineering of Hollow Core-Shell Interlinked Carbon Spheres for Highly Stable Lithium-Sulfur Batteries. *ACS Nano* **2015**, *9*, 8504−8513.
(17) Li, W.; Liang, Z.; Lu, Z.; Yao, H.; Seh, Z. W.; Yan, K.; Zheng, G.; Cui, Y. A Sulfur Cathode with Pomegranate-Like Cluster Structure. *Adv. Energy Mater.* **2015**, *5*, No. 1500211.
(18) Li, Z.; Zhang, J. T.; Chen, Y. M.; Li, J.; Lou, X. W. Pie-like Electrode Design for High-Energy Density Lithium-Sulfur Batteries. *Nat. Commun.* **2015**, *6*, No. 8850.
(19) Trofimov, B. A. Sulfurization of Polymers: A Novel Access to Electroactive and Conducting Materials. *Sulfur Rep.* **2003**, *24*, 283−305.
(20) Wang, J.; Yang, J.; Xie, J.; Xu, N. A Novel Conductive Polymer-Sulfur Composite Cathode Material for Rechargeable Lithium Batteries. *Adv. Mater.* **2002**, *14*, 963−965.
(21) Wang, J.; Yang, J.; Wan, C.; Du, K.; Xie, J.; Xu, N. Sulfur Composite Cathode Materials for Rechargeable Lithium Batteries. *Adv. Funct. Mater.* **2003**, *13*, 487−492.
(22) Fanous, J.; Wegner, M.; Spera, M. B. M.; Buchmeiser, M. R. High Energy Density Poly(Acrylonitrile)-Sulfur Composite-Based Lithium-Sulfur Batteries. *J. Electrochem. Soc.* **2013**, *160*, A1169−A1170.
(23) Fanous, J.; Wegner, M.; Grimminger, J.; Andresen, Ä.; Buchmeiser, M. R. Structure-Related Electrochemistry of Sulfur-Poly(Acrylonitrile) Composite Cathode Materials for Rechargeable Lithium Batteries. *Chem. Mater.* **2011**, *23*, 5024−5028.
(24) Fanous, J.; Wegner, M.; Grimminger, J.; Rolff, M.; Spera, M. B. M.; Tenzer, M.; Buchmeiser, M. R. Correlation of the Electrochemistry of Poly(Acrylonitrile)-Sulfur Composite Cathodes with Their Molecular Structure. *J. Mater. Chem.* **2012**, *22*, 23240−23245.
(25) Wang, W.; Cao, Z.; Elia, G. A.; Wu, Y.; Wahyudi, W.; Abou-Hamad, E.; Emwas, A. H.; Cavallo, L.; Li, L. J.; Ming, J. Recognizing the Mechanism of Sulfurized Polyacrylonitrile Cathode Materials for Li-S Batteries and beyond in Al-S Batteries. *ACS Energy Lett.* **2018**, *3*, 2899−2907.
(26) Wang, L.; Zhao, J.; He, X.; Wan, C. Kinetic Investigation of Sulfurized Polyacrylonitrile Cathode Material by Electrochemical Impedance Spectroscopy. *Electrochim. Acta* **2011**, *56*, 5252−5256.
(27) Liu, Y.; Haridas, A. K.; Cho, K. K.; Lee, Y.; Ahn, J. H. Highly Ordered Mesoporous Sulfurized Polyacrylonitrile Cathode Material for High-Rate Lithium Sulfur Batteries. *J. Phys. Chem. C* **2017**, *121*, 26172−26179.
(28) Yin, L.; Wang, J.; Yang, J.; Nuli, Y. A Novel Pyrolyzed Polyacrylonitrile-Sulfur@MWCNT Composite Cathode Material for High-Rate Rechargeable Lithium/Sulfur Batteries. *J. Mater. Chem.* **2011**, *21*, 6807−6810.
(29) Wang, W.; Cao, Z.; Elia, G. A.; Wu, Y.; Wahyudi, W.; Abou-Hamad, E.; Emwas, A. H.; Cavallo, L.; Li, L. J.; Ming, J. Recognizing the Mechanism of Sulfurized Polyacrylonitrile Cathode Materials for Li-S Batteries and beyond in Al-S Batteries. *ACS Energy Lett.* **2018**, *3*, 2899−2907.
(30) Fan, L.; Chen, S.; Zhu, J.; Ma, R.; Li, S.; Podila, R.; Rao, A. M.; Yang, G.; Wang, C.; Liu, Q.; Xu, Z.; Yuan, L.; Huang, Y.; Lu, B. Simultaneous Suppression of the Dendrite Formation and Shuttle Effect in a Lithium−Sulfur Battery by Bilateral Solid Electrolyte Interface. *Adv. Sci.* **2018**, *5*, No. 1700934.
(31) Peng, H. J.; Huang, J. Q.; Cheng, X. B.; Zhang, Q. Review on High-Loading and High-Energy Lithium−Sulfur Batteries. *Adv. Energy Mater.* **2017**, *7*, No. 1700260.
(32) Manthiram, A.; Chung, S. H.; Zu, C. Lithium-Sulfur Batteries: Progress and Prospects. *Adv. Mater.* **2015**, *27*, 1980−2006.
(33) Long, J. W.; Dunn, B.; Rolison, D. R.; White, H. S. Three-Dimensional Battery Architectures. *Chem. Rev.* **2004**, *104*, 4463−4492.
(34) Chung, S. H.; Manthiram, A. Lithium-Sulfur Batteries with Superior Cycle Stability by Employing Porous Current Collectors. *Electrochim. Acta* **2013**, *107*, 569−576.
(35) Chung, S. H.; Manthiram, A. Low-Cost, Porous Carbon Current Collector with High Sulfur Loading for Lithium-Sulfur Batteries. *Electrochem. Commun.* **2014**, *38*, 91−95.
(36) Zhang, Y.; Bakenov, Z.; Zhao, Y.; Konarov, A.; Wang, Q.; Chen, P. Three-Dimensional Carbon Fiber as Current Collector for Lithium/Sulfur Batteries. *Ionics* **2014**, *20*, 803−808.
(37) Cheng, X. B.; Peng, H. J.; Huang, J. Q.; Zhu, L.; Yang, S. H.; Liu, Y.; Zhang, H. W.; Zhu, W.; Wei, F.; Zhang, Q. Three-Dimensional Aluminum Foam/Carbon Nanotube Scaffolds as Long- and Short-Range Electron Pathways with Improved Sulfur Loading for High Energy Density Lithium-Sulfur Batteries. *J. Power Sources* **2014**, *261*, 264−270.
(38) Zhou, G.; Zhao, Y.; Manthiram, A. Dual-Confined Flexible Sulfur Cathodes Encapsulated in Nitrogen-Doped Double-Shelled Hollow Carbon Spheres and Wrapped with Graphene for Li-S Batteries. *Adv. Energy Mater.* **2015**, *5*, No. 1402263.
(39) Chung, S. H.; Chang, C. H.; Manthiram, A. A Carbon-Cotton Cathode with Ultrahigh-Loading Capability for Statically and Dynamically Stable Lithium-Sulfur Batteries. *ACS Nano* **2016**, *10*, 10462−10470.
(40) Zhou, G.; Li, L.; Ma, C.; Wang, S.; Shi, Y.; Koratkar, N.; Ren, W.; Li, F.; Cheng, H. M. A Graphene Foam Electrode with High Sulfur Loading for Flexible and High Energy Li-S Batteries. *Nano Energy* **2015**, *11*, 356−365.
(41) Liu, Y.; Zhu, Y.; Cui, Y. Challenges and Opportunities towards Fast-Charging Battery Materials. *Nat. Energy* **2019**, *4*, 540−550.
(42) Wild, M.; O'Neill, L.; Zhang, T.; Purkayastha, R.; Minton, G.; Marinescu, M.; Offer, G. J. Lithium Sulfur Batteries, a Mechanistic Review. *Energy Environ. Sci.* **2015**, *8*, 3477−3494.
(43) Wu, H. L.; Huff, L. A.; Gewirth, A. A. In Situ Raman Spectroscopy of Sulfur Speciation in Lithium-Sulfur Batteries. *ACS Appl. Mater. Interfaces* **2015**, *7*, 1709−1719.
(44) Jiang, M.; Wang, K.; Gao, S.; Wang, R.; Han, J.; Yan, J.; Cheng, S.; Jiang, K. Selenium as Extra Binding Site for Sulfur Species in Sulfurized Polyacrylonitrile Cathodes for High Capacity Lithium-Sulfur Batteries. *ChemElectroChem* **2019**, *6*, 1365−1370.
(45) Chen, X.; Peng, L.; Wang, L.; Yang, J.; Hao, Z.; Xiang, J.; Yuan, K.; Huang, Y.; Shan, B.; Yuan, L.; Xie, J. Ether-Compatible Sulfurized Polyacrylonitrile Cathode with Excellent Performance Enabled by Fast Kinetics via Selenium Doping. *Nat. Commun.* **2019**, *10*, No. 1021.
(46) Haran, B. S.; Durairajan, A.; Ramadass, P.; White, R. E.; Popov, B. N. In *Studies on Capacity Fade of Spinel Based Li-Ion Batteries*, Proceedings of the Intersociety Energy Conversion Engineering Conference; 2001; pp 935−940.
(47) Nagasubramanian, G. Two- and Three-Electrode Impedance Studies on 18650 Li-Ion Cells. *J. Power Sources* **2000**, *87*, 226−229.
(48) Andre, D.; Meiler, M.; Steiner, K.; Wimmer, C.; Soczka-Guth, T.; Sauer, D. U. Characterization of High-Power Lithium-Ion Batteries by Electrochemical Impedance Spectroscopy. I. Experimental Investigation. *J. Power Sources* **2011**, *196*, 5334−5341.
(49) Guo, J.; Sun, A.; Chen, X.; Wang, C.; Manivannan, A. Cyclability Study of Silicon-Carbon Composite Anodes for Lithium-

https://dx.doi.org/10.1021/acsanm.0c02073
ACS Appl. Nano Mater. 2021, 4, 53−60

Ion Batteries Using Electrochemical Impedance Spectroscopy. *Electrochim. Acta* **2011**, *56*, 3981−3987.
(50) Zegeye, T. A.; Kuo, C. F. J.; Wotango, A. S.; Pan, C. J.; Chen, H. M.; Haregewoin, A. M.; Cheng, J. H.; Su, W. N.; Hwang, B. J. Hybrid Nanostructured Microporous Carbon-Mesoporous Carbon Doped Titanium Dioxide/Sulfur Composite Positive Electrode Materials for Rechargeable Lithium-Sulfur Batteries. *J. Power Sources* **2016**, *324*, 239−252.
(51) Cheng, Q. Porous Graphene Sponge Additives for Lithium Ion Batteries with Excellent Rate Capability. *Sci. Rep.* **2017**, *7*, No. 925.
(52) Wu, Y.; Wang, W.; Ming, J.; Li, M.; Xie, L.; He, X.; Wang, J.; Liang, S.; Wu, Y. An Exploration of New Energy Storage System: High Energy Density, High Safety, and Fast Charging Lithium Ion Battery. *Adv. Funct. Mater.* **2019**, *29*, No. 1805978.

https://dx.doi.org/10.1021/acsanm.0c02073
ACS Appl. Nano Mater. 2021, 4, 53−60